Biophysical Journal, Volume 100

Supporting Material

Calcium dynamics in the ventricular myocytes of SERCA2 KO mice: a modelling study

Liren Li, William E Louch, Steven A Niederer, Kristin B Andersson, Geir Christensen, Ole M Sejersted, and Nicolas P Smith

Materials and Methods: Animal Care

All animal use was approved by the Norwegian National Committee for Animal Welfare under the Norwegian Animal Welfare Act, which conforms to with the *Guide for the Care and Use of Laboratory Animals* published by the US National Institutes of Health (NIH publication No. 85-23, revised 1996). The *Serca2*flox/flox Tg(αMHC-MerCreMer) mouse (KO) was employed, which allows for inducible, cardiomyocyte-specific disruption of the *Serca2* gene in adult mice (2). *Serca2* gene excision in 8-10 week old mice was accomplished by inclusion of taxomifen base powder (RM1 FG SQC, 811004, Scanbur BK) in the feed (100mg/200 g) for 7 days (1, 11). *Serca2*flox/flox mice (FF) served as controls (2, 3). Tamoxifen administration triggers *Serca2* gene excision exclusively in the cardiomyocytes of KO animals (2). Hearts were harvested at 4 weeks following tamoxifen treatment.

Parameterization

MATLAB (The MathWorks, Matick, MA) was used for all data analysis and parameter fitting. For parameter fitting, we used either a subspace trust region method ('lsqcurvefit' function) or the unconstrained nonlinear optimization function based on the Nelder-Mead Simplex Method ('fminsearch' function).

Intracellular Ca^{2+} buffering was accounted for using the equation proposed by Trafford et al. (17). Parameters for sarcolemmal Ca^{2+} fluxes, i.e. fluxes through NCX (J_{NCX}) and PMCA (J_{PMCA}), were fitted to the decay phase of the caffeine-induced $[Ca^{2+}]_i$ transient following field-stimulation at 1 Hz. The relative contributions of NCX and PMCA to sarcolemmal Ca^{2+} removal ($J_{sarcolemma}$) were determined based on previously published experimental observations by Li et al. (9). In indo 1-AM loaded mouse ventricular myocytes, using caffeine to block SR Ca^{2+} uptake and Na^+ and Ca^{2+}-free solution to block Ca^{2+} extrusion via NCX, and by analyzing the rate constants of decay of the $[Ca^{2+}]_i$ transients, the fractions of Ca^{2+} removed from the cytosol via SERCA, NCX and the slow mechanisms

(PMCA and mitochondria) were estimated to be 90.3, 9.2 and 0.5% respectively, or alternatively NCX and PMCA contributed to approximately 95 and 5% of sarcolemmal Ca^{2+} extrusion. Because indo 1 compartmentalization was thought to cause a possible underestimation of the slow mechanisms of Ca^{2+} extrusion, the above analysis was repeated using twitch relaxation data estimating the contributions of NCX and PMCA to be approximately 74 and 26% respectively (9). Based on these observations, we assigned 80 and 20% of $J_{sarcolemma}$ to J_{NCX} and J_{PMCA} respectively.

For fitting the KO data, a slight modification was introduced to account for the suspected change in the percentage contributions of NCX and PMCA to the sarcolemmal Ca^{2+} flux in the KO cardiomyocytes. Specifically, we set the maximum rate of J_{PMCA} in the KO model to be 145% of the fitted FF value, consistent with the percentage increase in its protein expression level observed experimentally. The affinity of PMCA to Ca^{2+} was assumed to be unchanged. The difference between $J_{sarcolemma}$ and the estimated J_{PMCA}, during the caffeine-induced $[Ca^{2+}]_i$ transient, was then attributed to J_{NCX} and used to fit the model of NCX.

Fig. S1 shows the process of parameterization of NCX in the FF and KO models. Representative caffeine-induced $[Ca^{2+}]_i$ transients recorded in the FF and KO cardiomyocytes are shown in Fig. S1A. The experimentally calculated total fluxes of Ca^{2+} through the sarcolemma and the corresponding fitted $J_{sarcolemma}$ are plotted as a function of Ca^{2+} in Fig. S1B. Using the fitted parameter values for NCX and PMCA, the decay of the $[Ca^{2+}]_i$ transients have been calculated and superimposed onto the experimental measurements in Fig. S1A. Our analysis of the decay of the caffeine-induced $[Ca^{2+}]_i$ transients showed that for the same level of $[Ca^{2+}]_i$, $J_{sarcolemma}$ was significantly greater in the KO compared to the FF. Based on the assumptions that NCX and PMCA contributed to 80 and 20% of Ca^{2+} extrusion respectively in the FF and that the functional activity of PMCA was increased by 45% in the

KO equivalent (2), the fitted value for the maximum exchange rate of NCX ($V_{NCX}^{\max}$) increased from 1.06 pA/pF in the FF Model to 3.63 pA/pF in the KO model. This corresponded to a 3.5-fold increase in the functional activity of NCX. Other fitted parameters governing the exchanger activity were not found to be significantly different from the FF model and thus were assumed to remain unchanged.

The fitted NCX and PMCA parameters were then used to predict $J_{sarcolemma}$ during field-stimulations at 1 and 6 Hz. $[Na^+]_i$ was set to be 10 and 15 mM at 1 and 6 Hz respectively, based on simulation results from the previously developed murine electrophysiology model at 35^{o}C (10) and are within the range of measured values (21). During the late phase (90 ms and 60 ms post-peak at 1 Hz and 6 Hz respectively) of the decay of the field-stimulated $[Ca^{2+}]_i$ transient, net Ca^{2+} uptake through SERCA (J_{SERCA}) was calculated as the difference between total Ca^{2+} flux (J_{total}) and the predicted $J_{sarcolemma}$, which was then used to fit the maximum uptake rate of SERCA (V_{up}), the Ca^{2+} affinity of the pump ($K_{m,up}$) and the SR Ca^{2+} leak flux (J_{leak}), yielding values of 0.162 μM/ms, 0.322 μM and 0.0088 μM/ms, respectively, at 1 Hz. The root mean square difference between fitted and measured J_{SERCA} was 3.04×10^{-4}. The rate of SR Ca^{2+} leak ($V_{leak} = 2 \times 10^{-5}$ ms^{-1}) in the model was then set such that SR Ca^{2+} leak flux in the whole-cell simulation was at the same level as the estimated J_{leak}.

At 6 Hz, J_{SERCA} was found to be significantly greater compared to 1 Hz, given the same level of $[Ca^{2+}]_i$. To account for this frequency-dependent acceleration of relaxation, V_{up} was re-fitted while setting $K_{m,up}$ to be the same as 1 Hz and J_{leak} (0.02 μM/ms) to be the simulated level when the model was paced at 6 Hz, yielding a V_{up} of 0.42 μM/ms with an RMSD of 1.2×10^{-3}. $K_{m,up}$ was assumed to remain unchanged at different pacing frequencies, based on the recently published finding that FDAR is a result of an increase in V_{up} without a change in its affinity to Ca^{2+} (14).

Similarly for the KO at 1 and 6 Hz, V_{up} had fitted values of 0.078 and 0.23 μM/ms respectively. J_{leak} had values of 0.0084 and 0.023 μM/ms respectively (V_{leak} = 6 × 10^{-3} ms^{-1}). Including $K_{m,up}$ in the fitting process at 1 Hz did not improve the quality of the fit (RMSD = 5.74 × 10^{-6} *vs* 5.88 × 10^{-6} for free $K_{m,up}$ *vs* fixed $K_{m,up}$). Therefore, $K_{m,up}$ (0.322 μM) was assumed to be unchanged between the FF and KO in the final model. The increase in V_{up} with increasing frequency was then incorporated into our framework using a simple phenomenological model of the CaMKII-regulatory pathway as previously(10), for both the FF and KO models.

The simulated and experimentally measured current-voltage relationship of the I_{CaL} for test potentials between -40 and 60 mV (see Materials and Methods) are shown in Fig. S2A. It can be seen that at test potentials between -20 and 20 mV, peak I_{CaL} current density during voltage clamp was greater in magnitude in the KO myocytes compared to the FF. The simulated and experimentally recorded time courses of the current at -10 mV test potential are shown in Fig. S2B. A list of all the parameters and their values are provided in Table S1.

Validation

Experimentally measured $[Ca^{2+}]_i$ transients in the FF and KO myocytes at pacing frequencies of 1 and 6 Hz (Fig. 2A and C) were compared with simulation results at these frequencies (Fig. 2B and D). Key characteristics are summarized in Table 1. At 1 Hz, simulated diastolic $[Ca^{2+}]_i$ in the FF and KO models were similar, consistent with experimental measurements. $\Delta[Ca^{2+}]_i$ was decreased in the KO model by 88% and RT_{50} increased by 105% from the FF values, compared with changes of 85 and 118% measured experimentally. At 6 Hz, simulated diastolic $[Ca^{2+}]_i$ in the FF and KO models were again very similar, consistent with experimental measurements. Simulated $\Delta[Ca^{2+}]_i$ in the KO model was decreased by 74% from the FF value, compared to 75% measured experimentally. This was paralleled by an increased RT_{50} in both the model and experimental measurements (30 and 20%

increase, respectively). It is worth noting that at the more physiological frequency of 6 Hz, the decrease in the rate of decay of the $[Ca^{2+}]_i$ transient in the KO model was less pronounced than at 1 Hz, as indicated by the significantly smaller percentage change in RT_{50} between KO and FF models. Simulated SR Ca^{2+} contents in the KO and FF models at 0.5 Hz were 8.2 and 61.0 μmol per L cytosol, respectively, corresponding to an 87% reduction in SR Ca^{2+} loading. This is consistent with the 87% reduction in the magnitude of the caffeine-induced $[Ca^{2+}]_i$ transient observed experimentally in the KO cardiomyocytes.

The contribute on of the SR to the $[Ca^{2+}]_i$ transient can be estimated experimentally from the difference in the magnitudes of the transients before and during sustained caffeine treatment. By this method, the contribution of SR to the transient was estimated to be 88% in the FF cardiomyocytes and 30% in the KO cardiomyocytes at 0.5 Hz. In our model, SR contribution could be calculated more directly as the ratio between the integral of J_{SERCA} and the integral of the sum of the removal fluxes through SERCA, NCX and PMCA over one cardiac cycle. The integral of these Ca^{2+} removal fluxes at 0.5 Hz are shown in Fig. 2 E-G. The percentage contribution of SERCA to Ca^{2+} removal was 86% in the FF model and 36% in the KO model, consistent with experimental estimates. The contributions of NCX in the FF and KO models were 12% and 58% respectively, while the contributions of PMCA were 2 and 6% respectively.

Detailed Quantitative Analysis of Changes in Ca^{2+} Handling with SERCA2 KO

Simulated APs elicited by field-stimulation at 1 and 6 Hz are plotted in Fig. S3A and B, respectively. At the lower pacing frequency of 1 Hz, there was a slight prolongation in late repolarization in the KO model, with the time to 90% (APD_{90}) repolarization equal to 24.4 ms, compared to 18.9 ms respectively in the FF model. At the higher pacing frequency of 6 Hz, repolarization was faster compared to the same model at 1 Hz and the differences in action potential durations between the

models were diminished, with the APD_{50} equal to 12.2 and 13.1 ms respectively.

Simulated time courses of the I_{CaL} during the above APs are plotted in Fig. S3C and D, showing an enhanced I_{CaL} in the KO model, with both greater magnitude and slower inactivation kinetics. At 1 Hz (Fig. S3C), maximum current density increased from 15.6 pA/pF in the FF model to 17.5 pA/pF in the KO model. The integral of the current over the duration of the action potential was 0.12 pC/pF in the FF model and 0.16 pC/pF in the KO model. Similarly at 6 Hz (Fig. S3D), the integral of the current increased by 49% in the KO model.

Simulated net fluxes of Ca^{2+} uptake through SERCA (J_{SERCA}) are shown in Fig. S3E and F for one cardiac cycle at 1 and 6 Hz, respectively (note difference in figure scale for FF and KO). At 1 Hz, peak J_{SERCA} during systole in the KO model was 0.015 μMms, compared to 0.14 μM/ms in the FF model, corresponding to an 89% decrease in systolic SERCA activity. During diastole, J_{SERCA} in the KO model was 0.0036 μMms compared to 0.0094 μM/ms in the FF model, corresponding to a 62% decrease in diastolic SERCA activity. The total amount of Ca^{2+} uptake, calculated as the integral of J_{SERCA} over one cardiac cycle, decreased from 49.2 μM in the FF model to 7.4 μM in the KO model, corresponding to an 85% decrease. At 6 Hz with SERCA2 KO, J_{SERCA} decreased by 73 and 61% of control values during systole and diastole respectively, and total Ca^{2+} uptake decreased by 71%.

Simulated fluxes of Ca^{2+} through NCX (J_{NCX}) are plotted in Fig. S3G and H for 1 and 6 Hz, respectively. During an action potential, there is a very brief period where Ca^{2+} influx via NCX is thermodynamically favored. This Ca^{2+} influx, corresponding to positive values of J_{NCX}, was greater in the KO model compared to FF model. At 1 Hz, the magnitude of the influx was relatively small, equal to 0.0018 μM/ms in the FF model and increasing 5-fold to 0.0089 μM/ms in the KO model. At 6 Hz, the elevation of $[Na^+]_i$ resulted in an enhanced Ca^{2+} influx through reverse mode NCX. Peak Ca^{2+}

influx was 0.0055 μM/ms in the FF model and increased 3.6-fold to 0.020 μM/ms in the KO model. These results show that Ca^{2+} entry through reverse mode NCX was significantly enhanced in the KO model, although its magnitude was relatively small compared to Ca^{2+} entry through I_{CaL}.

When comparing Ca^{2+} extrusion through NCX in forward mode, J_{NCX} in the KO model was lower during systole and higher during diastole compared to the FF model. Quantitative analysis showed that peak systolic J_{NCX} in the KO model was 0.011 μM/ms compared to 0.017 μM/ms in the FF model, corresponding to a 35% decrease. This moderate reduction in NCX activity occurred despite a 73% decrease in peak $[Ca^{2+}]_i$. Diastolic J_{NCX} was 0.0041 μM/ms in the KO model compared to 0.0009 μM/ms in the FF model, corresponding to a 4.5-fold increase. At 6 Hz, both systolic and diastolic J_{NCX} was higher in the KO model. During systole, J_{NCX} was 0.009 μM/ms in the KO model compared to 0.007 μM/ms in the FF model corresponding to a 33% increase. During diastole, J_{NCX} was 0.0052 μM/ms in the KO model compared to 0.0019 in the FF model corresponding to a 2.5-fold increase.

Theoretical Analysis of the decay of the $[Ca^{2+}]_i$ transient

Assuming that Ca^{2+} transport by SERCA is the min contributor to $[Ca^{2+}]_i$ decline, the rate of decay of the total Ca^{2+} concentration in the cytosol ($[Ca^{2+}]_{tot}$) can be written as

$$\frac{d[Ca^{2+}]_{tot}}{dt} = J_{SERCA} = \frac{-V_{up}}{1+(K_{m,up}/[Ca^{2+}]_i)^2} \qquad \text{(S1)}$$

$[Ca^{2+}]_{tot}$ is related to $[Ca^{2+}]_i$by the buffering equation:

$$[Ca^{2+}]_{tot} = [Ca^{2+}]_i + \frac{B_{\max}}{1+K_d/[Ca^{2+}]_i} \qquad \text{(S2)}$$

where B_{max} and K_d are the maximum binding capacity and overall binding affinity of the buffers. Eqs. S1 and S2 can be combined to give the rate of decay of $[Ca^{2+}]_i$:

$$\frac{d[Ca^{2+}]_i}{dt} = \frac{-V_{up} \cdot [Ca^{2+}]_i \cdot (1 + K_d / [Ca^{2+}]_i)^2}{K_d \cdot B_{\max} \cdot [1 + (K_{m,up} / [Ca^{2+}]_i)^2]} \quad \text{(S3)}$$

Rearranging Eq. S3 and integrating gives Eq. (1).

The results presented in Fig. 6 demonstrate a much greater shift in RT_{50} at 1 Hz compared to 6 Hz, consistent with experimental observations and our model results. However, it is interesting to note that, with a more simplistic model framework (6) which did not include FDAR, Trafford et al. (18) were able to demonstrate the reduced lusitropic effect of SERCA KO at 6 Hz. To explain this result using the approach of Bers and Berlin (ref. 22, in the main paper), we ran the FF and KO models with a constant V_{up} value, set to its level at 1 Hz. The decay of the simulated $[Ca^{2+}]_i$ transients at 6 Hz were slower in both the FF and KO models, compared to the case with FDAR (FF: 59 *vs* 48 ms, KO: 68 *vs* 60 ms), as a consequence of the slower SERCA uptake rate. However, the difference in RT_{60} between the FF and KO models remained smaller at 6 Hz than at 1 Hz (6 Hz: 59 *vs* 68 ms, 1 Hz: 119 *vs* 267 ms). Substituting the appropriate parameter values into Equation (1) yielded a qualitatively similar relationship (Fig. S4) between RT_{50} and peak $[Ca^{2+}]_i$ as that in Fig. S4. This result indicates that the reduced lusitropic impact of SERCA KO at a higher pacing frequency may not involve FDAR.

Sensitivity of the rate of $[Ca^{2+}]_i$ decay to buffering parameters

The analysis outlined in the previous section is applied to test the sensitivity of RT_{50} to changes in the buffering parameters. B_{max} was varied from 60 to 160 μM and K_d from 0.3 to 1.6 μM. Analyses of the RT_{50} with the range of B_{max} and K_d values are shown in Fig. S5 and Fig. S6, respectively.

Limitations

In the process of parameterizing the NCX and PMCA formulations in the KO model, we have separated these two Ca^{2+} fluxes during the decay of the caffeine-induced Ca^{2+} transient based on the

assumption that a 45% increase in PMCA expression level observed experimentally led to the same percentage increase in its activity. The validity of this assumption requires further investigation, such as an additional experiment of a caffeine-induced $[Ca^{2+}]_i$ transient in the presence of an NCX inhibitor. Nevertheless, we tested the sensitivity of our model results to changes in the ratio between J_{NCX} and J_{PMCA} in the KO model. The key finding that NCX up-regulation was important for maintaining diastolic $[Ca^{2+}]_i$ in the KO model was not found to be sensitive to the above assumption.

In our model, SERCA activities in the FF and KO cardiomyocytes were obtained from analyzing the decay of field-stimulated $[Ca^{2+}]_i$ transients at 1 and 6 Hz. While the analysis is based on the assumptions of no changes in buffering properties and negligible mitochondrial Ca^{2+} transport, the method has been consistently validated and represents the standard method for functionally characterizing Ca^{2+} uptake through SERCA. For example, Shannon et al. (15) used this method in their study of $[Ca^{2+}]_i$ decline in voltage-clamped rabbit ventricular myocytes. Picht et al. (14) used the same method for characterizing the frequency-dependent changes in SERCA activity in mouse ventricular myocytes. Li et al. (9) also characterized Ca^{2+} transport in phospholamban knockout mouse using this method. Additional examples supporting the validity of our approach can be found in many other studies (12, 13, 16, 19). Studies using SR vesicles prepared from cardiac tissue can provide an alternative method to characterize SERCA function (7). However, these preparations compromise the cellular environment and thus also the complex regulatory mechanisms. Therefore, results from these studies require careful interpretation and can not readily provide a quantitative relationship between protein density and function.

In our model, intracellular Ca^{2+} buffering was accounted for using the framework of rapid equilibrium approximation developed by Wagner and Keizer (20) and fitted by Trafford and Eisner (17) to data obtained from ferret ventricular myocytes at room temperature. The validity of the rapid equilibrium

approximation has been examined in detail by Wagner and Keizer (20), and has since been widely applied and acknowledged as a reasonable approximation to buffering properties in studies of Ca^{2+} handling (4, 9, 14). We have chosen this approach as a kinetic buffering model would involve additional parameters that can not be sufficiently constrained from available experimental data.

It was also assumed in the current study that intracellular Ca^{2+} buffering was unchanged with SERCA2 KO, although the reductions in the expression and activity of SERCA may result in a decrease in the overall Ca^{2+} buffering properties. Such a decrease would mean a decrease in the change of the total Ca^{2+} concentration for the same level of change in $[Ca^{2+}]_i$. This means that during the decay phase of the $[Ca^{2+}]_i$ transient, less Ca^{2+} would need to be removed from the cytosol to achieve the same decrease in $[Ca^{2+}]_i$. Under such circumstances, the activities of Ca^{2+} removal mechanisms may be overestimated in the current KO model. To investigate whether this could fully explain the proportionally higher SERCA activity found in our study, we tested how much buffering would need to change to yield an 85% reduction in SERCA activity as measured in myocardial tissue homogenate (2). The result was a 62% reduction in the maximum buffering activity, which is significantly greater than the reported total percentage contribution (approximately 19%) of SERCA to total buffering (5). In addition, the situation is further complicated by the possible alterations in the Ca^{2+} binding properties of the myofilaments, as mentioned previously, since troponin C is another important fast Ca^{2+} buffer with a similar Ca^{2+} binding affinity to SERCA, and contributes to approximately 46 and 29% of fast and total buffering respectively (5, 8). Furthermore, our sensitivity study on the rate of decay of the transient suggests that the reduced lusitropic effect of SERCA KO at a higher pacing frequency is independent of the choice of buffering parameters.

Parameter Definition and Values

Table S1: Parameter definitions and values

Parameter	*Definition*	*FF Value*	*KO value*
C_m	Specific membrane capacitance (μF/cm$^{2)}$	1.0	1.0
F	Faraday constant (C/mmol)	96.5	96.5
T	Absolute temperature (K)	310	310
R	Ideal gas constant (J/mol K)	8.314	8.314
A_{cap}	Capacitive membrane area (cm$^{2)}$	1.48×10^{-4}	1.55×10^{-4}
V_{myo}	Myoplasmic volume (μL)	2.2×10^{-5}	2.2×10^{-5}
V_{JSR}	Juctional SR volume (μL)	7.7×10^{-8}	7.7×10^{-8}
V_{NSR}	Network SR volume (μL)	2.31×10^{-7}	2.31×10^{-7}
V_{ds}	Dyadic space volume (μL)	2.2×10^{-8}	2.2×10^{-8}
B_{max}	Max. buffering capacity (μM)	109	109
Kd_{buffer}	Affinity of buffer to Ca^{2+} (μM)	0.6	0.6
$V_{NCX}^{\max}$	NCX: max. exchange rate (pA/pF)	1.059	3.626
$K_{m,Cao}$	NCX: affinity to extracellular Ca^{2+} (mM)	1.4	1.4
$K_{m,Cai}$	NCX : affinity to intracellular Ca^{2+} (mM)	0.0036	0.0036
$K_{m,Nai}$	NCX : affinity to intracellular Na^{+}	12	12
k_{sat}	NCX: saturation factor	0.27	0.27
η	NCX: V-dependence factor	0.35	0.35
K_{mallo}	NCX: allosteric regulation (μM)	0.142	0.142
f_o	CaMKII: initial fractional occupancy (%)	5	5
$K_{m,CaM}$	CaMKII: $[Ca^{2+}]_i$ for half activation (μM)	0.7	0.7
α	CaMKII: autophosphorylation rate (ms^{-2})	0.05	0.05
β	CaMKII: dephosphorylation rate (ms^{-1})	0.0002	0.0002
$K_{m,up}$	SERCA : affinity to Ca^{2+} μM	0.322	0.322
$\overline{V_{up}}$	SERCA: max. uptake rate in the absence of CaMKII (μM/ms)	0.0785	0.0017

Continued on next page

Table S1: continued from previous page

Parameter	Definition	FF value	KO value
$K_{m,CaMK}$	SERCA: half-saturation coefficient for CaMKII	0.819	0.690
n_{CaMK}	SERCA: Hill coefficient for interaction with CaMKII	11.97	17.86
nH	SERCA: Hill coefficient for binding to Ca^{2+}	2	2
$\overline{\Delta V_{up,CaMK}}$	SERCA: max. CaMKII-dependent increase in V_{up}	8.08	13.73
V_{leak}	SR leak: rate constant (ms^{-1})	2×10^{-5}	6×10^{-5}
P_{CaL}	LCC: permeability of the channel (ms^{-1})	9.5	8.5
Φ_L	LCC: proportion of time closed in open mode	2.5	2.5
t_L	LCC: time switching between C and O states (ms)	3	3
V_L	LCC: potential when half LCC open (mV)	-5	-5
ΔV_L	LCC: width of opening potentials (mV)	9	9
K_L	LCC: concentration at inactivation (μM)	0.25	0.23
τ_L	LCC: inactivation time (ms)	885.7	885.7
a	LCC: biasing to make inactivation function of V	0.3	0.3
b	LCC: biasing to make inactivation function of V	0.4	0.4
C_1	LCC: V-dependent inactivation constant 1 (mV)	33	33
C_2	LCC: V-dependent inactivation gate constant 2 (mV)	8.2	8.2
C_3	LCC: V-dependent inactivation gate constant 3 (ms)	0.1	0.1
C_4	LCC: V-dependent inactivation gate constant 4 (mV)	40	40
C_5	LCC: V-dependent inactivation gate constant 5 (mV)	6	6
C_6	LCC: V-dependent inactivation gate constant 6 (ms)	3	3
C_7	LCC: V-dependent inactivation gate constant 7 (ms)	315	315
C_8	LCC: V-dependent inactivation gate constant 8 (mV)	30	19
C_9	LCC: V-dependent inactivation gate constant 9 (mV)	5	2.7
$G_{kto,f}$	$I_{kto,f}$: max. conductance of the channel (mS/μF)	0.535	0.535
G_{kur}	I_{kur}: max. conductance of the channel (mS/μF)	0.250	0.250
G_{kss}	I_{kss}: max. conductance of the channel (mS/μF)	0.060	0.060
G_{kr}	I_{kr}: max. conductance of the channel	0.0165	0.0165

Continued on next page

Table S1: continued from previous page

Parameter	Definition	FF value	KO value
G_{ks}	I_{ks}: max. conductance of the channel	0.00575	0.00575
G_{K1}	I_{k1}: max. conductance of the channel	0.35	0.35
V_{rel}	RyR: max. Ca^{2+} permeability	4.5	4.5
k_a^+	RyR: $P_{C1} - P_{O1}$ rate constant (μM^{-4}/ms)	0.006075	0.006075
k_a^-	RyR: $P_{O1} - P_{C1}$ rate constant (ms^{-1})	0.0713	0.0713
k_b^+	RyR: $P_{O1} - P_{O2}$ rate constant (μM^{-3}/ms)	0.00405	0.00405
k_b^-	RyR: $P_{O2} - P_{O1}$ rate constant (ms^{-1})	0.965	0.965
k_c^+	RyR: $P_{O1} - P_{C2}$ rate constant (ms^{-1})	0.009	0.009
k_c^-	RyR: $P_{C2} - P_{O1}$ rate constant (ms^{-1})	0.0008	0.0008
n	RyR: Ca^{2+} cooperativity parameter $P_{C1} - P_{O1}$	4	4
m	RyR: Ca^{2+} cooperativity parameter $P_{O1} - P_{O2}$	3	3
$A_{P_{RyR}}$	P_{RyR}: Ca^{2+} release modulating constant A (ms^{-1})	-0.04	-0.04
$B_{P_{RyR}}$	P_{RyR}: Ca^{2+} release modulating constant B (ms^{-1})	-3.0	-3.0
τ_{tr}	Time constant for transfer from NSR to JSR (ms)	20.0	20.0
τ_{xfer}	Time constant for transfer from dyadic space to myoplasm (ms)	6.0	6.0
$CSQN_{tot}$	CSQN: Total concentration in JSR (mM)	50	50
K_m^{CSQN}	CSQN: Affinity to Ca^{2+} (mM)	0.63	0.63
$K_{m,Na}$	Na^+/K^+ pump: Affinity to Na^+ (mM)	16.6	16.6
I_{NaK}^{max}	Na^+/K^+ pump: Max. exchange current (pA/pF)	2.486	2.486
$K_{m,PMCA}$	PMCA: Affinity of the pump to Ca^{2+} (μM)	0.451	0.451
I_{PMCA}^{max}	PMCA: Max. pump current (pA/pF)	0.130	0.188
G_{Cab}	I_{Cab}: Max. conductance of the channel (mS/μF)	0.00022	0.00022

Continued on next page

Table S1: continued from previous page

Parameter	Definition	FF value	KO value
G_{Na}	$I_{Na:}$ Max. conductance of the channel (mS/μF)	25	25
G_{Nab}	$I_{Nab:}$ Max. conductance of the channel (mS/μF)	0.0026	0.0026
$G_{Cl,Ca}$	$I_{Cl,Ca}$: Max. conductance of the channel (mS/μF)	10.0	10.0
$K_{m,Cl}$	$I_{Cl,Ca}$: half saturation constant for the current (μM)	10.0	10.0
E_{Cl}	$I_{Cl,Ca}$: Reversal potential for the current (mV)	-40	-40

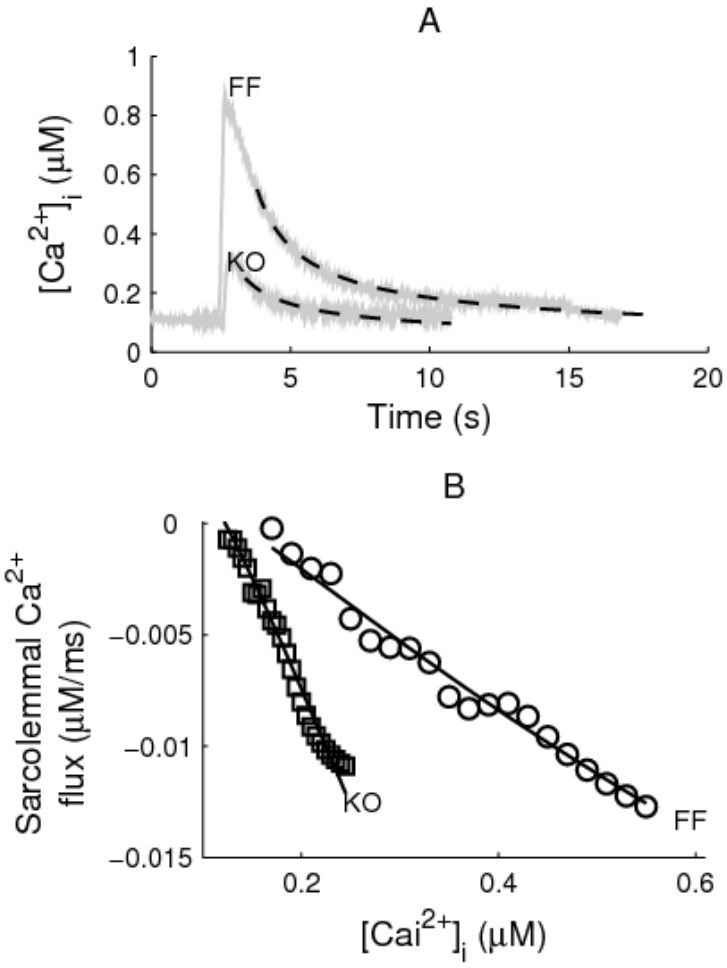

Figure S1: Parameterization of NCX in the FF and KO models. A: Average experimentally recorded caffeine-induced $[Ca^{2+}]_i$ transients in isolated ventricular myocytes from the SERCA2 FF and KO mice as indicated. Simulated decay of the $[Ca^{2+}]_i$ transients (dashed lines) using the fitted parameter values for NCX and PMCA are superimposed. B: The experimentally calculated total fluxes of Ca^{2+} through the sarcolemma ($J_{sarcolemma}$) plotted as a function of $[Ca^{2+}]_i$ obtained from the FF myocytes (circles) and KO myocytes (squares). The fitted $J_{sarcolemma}$ in the FF model (solid line) and KO model (dashed line) are superimposed.

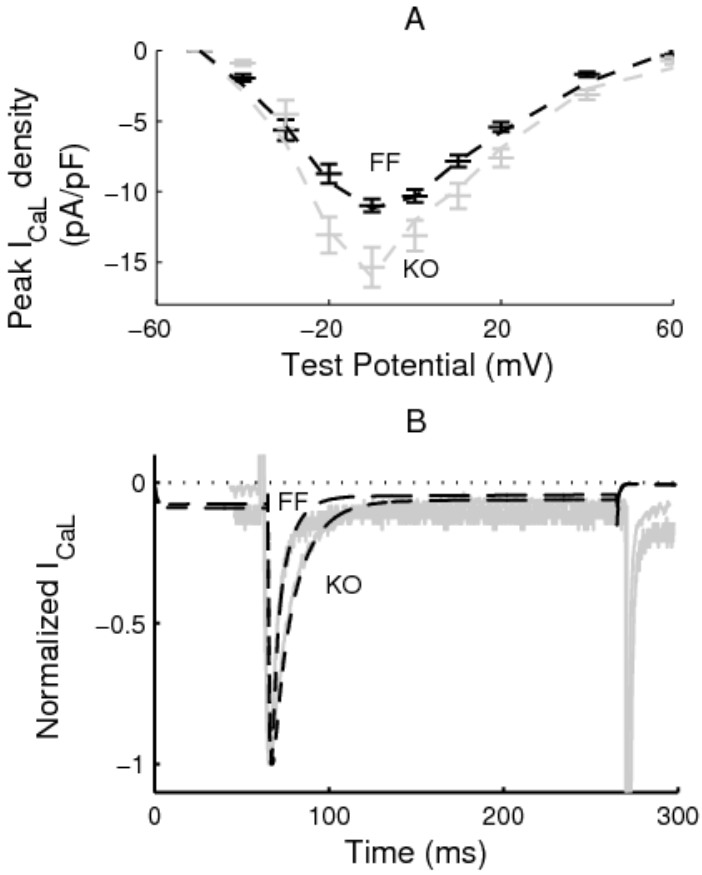

Figure S2: Parameterization of the L-type Ca^{2+} current (I_{CaL}). A: Experimentally recorded current-voltage relationship of I_{CaL} for test potentials between -40 and 60 mV (see Materials and Methods) in the FF (black) and KO (grey) myocytes. The fitted I-V relationship (dotted lines) is superimposed. B: The time courses of the I_{CaL} at the test potential of -10 mV, showing slower inactivation kinetics with SERCA2 KO with the time constant (τ) of decay increasing from 5.5 ms in the FF myocytes to 12.8 ms in the KO myocytes. The fitted time courses (dotted lines) are superimposed.

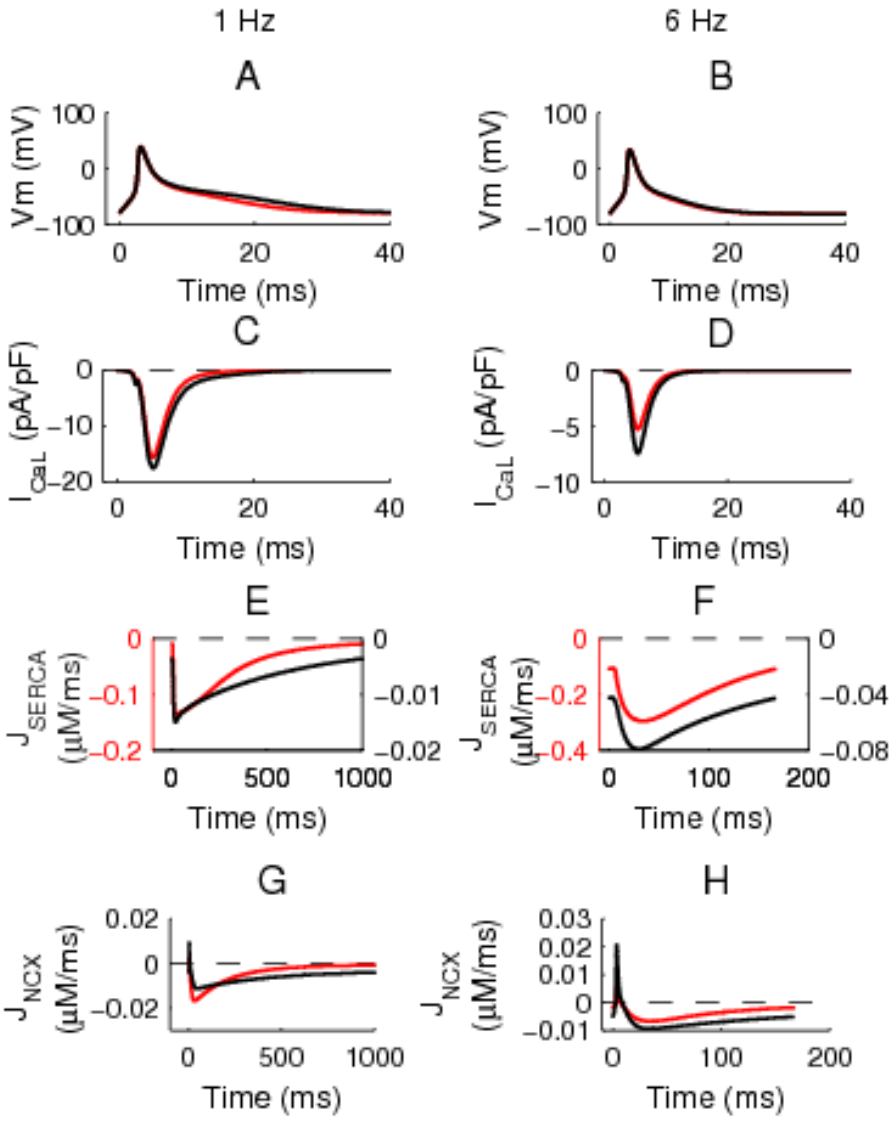

Figure S3: Simulated Ca^{2+} dynamics in the FF (red) and KO (black) models at 1 and 6 Hz. A-B: Simulated AP at 1 (A) and 6 Hz (B) . C-D: Simulated time courses of I_{CaL} at 1 (C) and 6 Hz (D). E-F: Simulated time courses of Ca^{2+} uptake through SERCA (J_{SERCA}) at 1 (E) and 6 Hz (F). G-H: Simulated time courses of Ca^{2+} extrusion through NCX (J_{NCX}) at 1 (G) and 6 Hz (H).

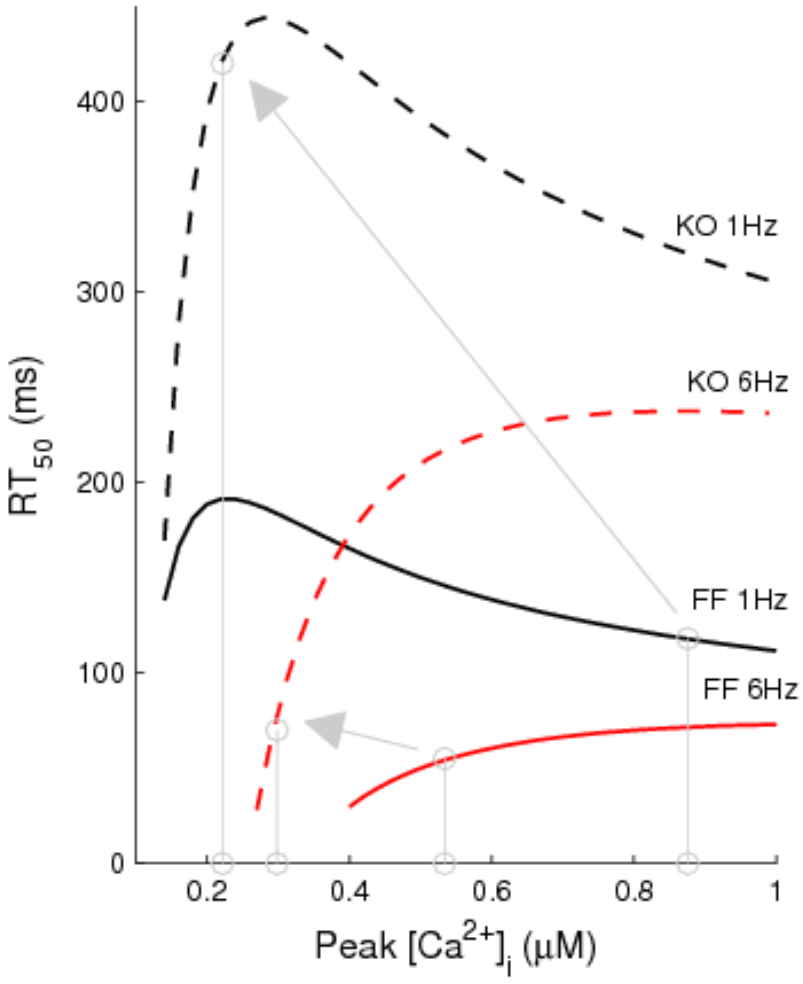

Figure S4: Analysis of the RT_{50} of $[Ca^{2+}]_i$ transients in the FF and KO models without FDAR. The circles corresponding to the simulated peak $[Ca^{2+}]_i$ and the predicted RT_{50} values.

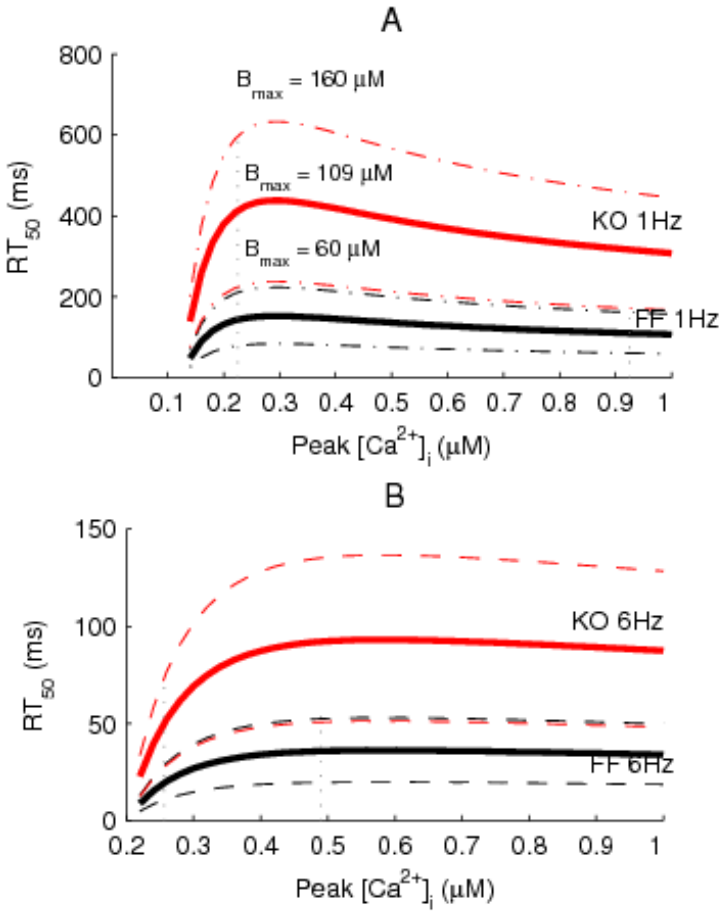

Figure S5: Analysis of the RT_{50} of $[Ca^{2+}]_i$ transients in the FF and KO models at 1 (A) and 6 (B) Hz, with a range of B_{max} values.

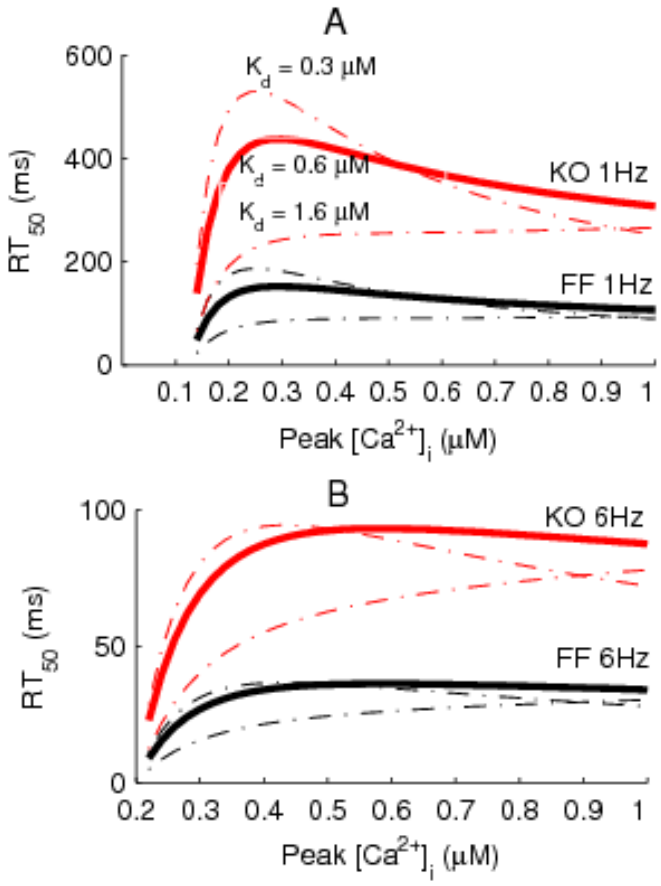

Figure S6: Analysis of the RT_{50} of $[Ca^{2+}]_i$ transients in the FF and KO models at 1 (A) and 6 (B) Hz, with a range of K_d values.

References

1. **Andersson K, Winer L, Mørk H, Molkentin J, and Jaisser F**. Tamoxifen administration routes and dosage for inducible Cre-mediated gene disruption in mouse hearts. *Transgenic Research* 19: 715-725, 2010.
2. **Andersson KB, Birkeland JAK, Finsen AV, Louch WE, Sjaastad I, Wang Y, Chen J, Molkentin JD, Chien KR, Sejersted OM, and Christensen G**. Moderate heart dysfunction in mice with inducible cardiomyocyte-specific excision of the Serca2 gene. *Journal of Molecular and Cellular Cardiology* 47: 180-187, 2009.
3. **Andersson KB, Finsen AV, Sjåland C, Winer LH, Sjaastad I, Ødegaard A, Louch WE, Wang Y, Chen J, Chien KR, Sejersted OM, and Christensen G**. Mice carrying a conditional Serca2flox allele for the generation of Ca2+ handling-deficient mouse models. *Cell Calcium* 46: 219-225, 2009.
4. **Berlin JR, Bassani JW, and Bers DM**. Intrinsic cytosolic calcium buffering properties of single rat cardiac myocytes. *Biophysical Journal* 67: 1775-1787, 1994.
5. **Bers DM**. *Excitation-Contraction Coupling and Cardiac Contractile Force*. Boston: Kluwer Academic Publishers, 2001.
6. **Bondarenko VE, Szigeti GP, Bett GCL, Kim S-J, and Rasmusson RL**. Computer model of action potential of mouse ventricular myocytes. *Am J Physiol Heart Circ Physiol* 287: H1378-1403, 2004.
7. **Currie S, and Smith GL**. Enhanced phosphorylation of phospholamban and downregulation of sarco/endoplasmic reticulum Ca2+ ATPase type 2 (SERCA 2) in cardiac sarcoplasmic reticulum from rabbits with heart failure. *Cardiovascular Research* 41: 135-146, 1999.
8. **Gao W, Backx P, Azan-Backx M, and Marban E**. Myofilament Ca2+ sensitivity in intact versus skinned rat ventricular muscle. *Circ Res* 74: 408-415, 1994.
9. **Li L, Chu G, Kranias EG, and Bers DM**. Cardiac myocyte calcium transport in phospholamban knockout mouse: relaxation and endogenous CaMKII effects. *Am J Physiol Heart Circ Physiol* 274: H1335-1347, 1998.
10. **Li L, Niederer SA, Idigo W, Zhang YH, Swietach P, Casadei B, and Smith NP**. A mathematical model of the murine ventricular myocyte: a data-driven biophysically based approach applied to mice overexpressing the canine NCX isoform. *Am J Physiol Heart Circ Physiol* 299: H1045-1063, 2010.
11. **Louch WE, Hougen K, MÃ¸rk HK, Swift F, Aronsen JM, Sjaastad I, Reims HM, Roald B, Andersson KB, Christensen G, and Sejersted OM**. Sodium accumulation promotes diastolic dysfunction in end-stage heart failure following Serca2 knockout. *The Journal of Physiology* 588: 465-478, 2010.
12. **Loughrey CM, Smith GL, and MacEachern KE**. Comparison of Ca2+ release and uptake characteristics of the sarcoplasmic reticulum in isolated horse and rabbit cardiomyocytes. *Am J Physiol Heart Circ Physiol* 287: H1149-1159, 2004.
13. **Piacentino V, III, Weber CR, Chen X, Weisser-Thomas J, Margulies KB, Bers DM, and Houser SR**. Cellular Basis of Abnormal Calcium Transients of Failing Human Ventricular Myocytes. *Circ Res* 92: 651-658, 2003.
14. **Picht E, DeSantiago J, Huke S, Kaetzel M, A, Dedman J, R, and Bers D, M.** . CaMKII inhibition targeted to the sarcoplasmic reticulum inhibits frequency-dependent acceleration of relaxation and Ca2+ current facilitation. *Journal of Molecular and Cellular Cardiology* 42: 196-205, 2007.
15. **Shannon TR, Ginsburg KS, and Bers DM**. Reverse Mode of the Sarcoplasmic Reticulum Calcium Pump and Load-Dependent Cytosolic Calcium Decline in Voltage-Clamped Cardiac Ventricular Myocytes. *Biophysical Journal* 78: 322-333, 2000.

16. **Teucher N, Prestle J, Seidler T, Currie S, Elliott EB, Reynolds DF, Schott P, Wagner S, Kogler H, Inesi G, Bers DM, Hasenfuss G, and Smith GL**. Excessive Sarcoplasmic/Endoplasmic Reticulum Ca2+-ATPase Expression Causes Increased Sarcoplasmic Reticulum Ca2+ Uptake but Decreases Myocyte Shortening. *Circulation* 110: 3553-3559, 2004.
17. **Trafford AW, Diaz ME, and Eisner DA**. A novel, rapid and reversible method to measure Ca buffering and time-course of total sarcoplasmic reticulum Ca content in cardiac ventricularm myocytes. *Pflugers Archiv European Journal of Physiology* 437: 501-503, 1999.
18. **Trafford AW, Lederer WJ, and Sobie EA**. Keeping the beat: Life without SERCA -- Is it possible? *Journal of Molecular and Cellular Cardiology* 47: 171-173, 2009.
19. **Waggoner JR, Ginsburg KS, Mitton B, Haghighi K, Robbins J, Bers DM, and Kranias EG**. Phospholamban overexpression in rabbit ventricular myocytes does not alter sarcoplasmic reticulum Ca transport. *Am J Physiol Heart Circ Physiol* 296: H698-703, 2009.
20. **Wagner J, and Keizer J**. Effects of rapid buffers on Ca2+ diffusion and Ca2+ oscillations. *Biophysical Journal* 67: 447-456, 1994.
21. **Yao A, Su Z, Nonaka A, Zubair I, Lu L, Philipson KD, Bridge JHB, and Barry WH**. Effects of Overexpression of the Na+-Ca2+ Exchanger on [Ca2+]i Transients in Murine Ventricular Myocytes. *Circ Res* 82: 657-665, 1998.